Ensemble-Based Analysis of Factors Leading to the Development of a Multiday Warm-Season Heavy Rain Event*

RUSS S. SCHUMACHER

Department of Atmospheric Sciences, Texas A&M University, College Station, Texas

(Manuscript received 29 October 2010, in final form 24 February 2011)

ABSTRACT

This study makes use of operational global ensemble forecasts from the European Centre for Medium-Range Weather Forecasts (ECMWF) to examine the factors contributing to, or inhibiting, the development of a long-lived continental vortex and its associated rainfall. From 25 to 30 June 2007, a vortex developed and grew upscale over the southern plains of the United States. It was associated with persistent heavy rainfall, with over 100 mm of rain falling in much of Texas, Oklahoma, Kansas, and Missouri, and amounts exceeding 300 mm in southeastern Kansas. Previous research has shown that, in comparison with other rainfall events of similar temporal and spatial scales, this event was particularly difficult for numerical models to predict.

Considering the ensemble members as different possible realizations of the evolution of the event, several methods are used to examine the processes that led to the development and maintenance of the long-lived vortex and its associated rainfall, and to its apparently limited predictability. Linear statistics are calculated to identify synoptic-scale flow features that were correlated to area-averaged precipitation, and differences between composites of ''dry'' and ''wet'' ensemble members are used to pinpoint the processes that were favorable or detrimental to the system's development. The maintenance of the vortex, and its slow movement in the southern plains, are found to be closely related to the strength of a closed midlevel anticyclone in the southwestern United States and the strength of a midlevel ridge in the northern plains. In particular, with a weaker upstream anticyclone, the shear and flow over the incipient vortex are relatively weak, which allows for slow movement and persistent heavy rains. On the other hand, when the upstream anticyclone is stronger, there is stronger northerly shear and flow, which causes the incipient vortex to move southwestward into the high terrain of Mexico and dissipate. These relatively small differences in the wind and mass fields early in the ensemble forecast, in conjunction with modifications of the synoptic and mesoscale flow by deep convection, lead to very large spread in the resulting precipitation forecasts.

1. Introduction

a. Overview

In late June and early July of 2007, persistent heavy rains fell on much of the southern Great Plains of the United States (Fig. 1). During this period of time, the primary synoptic-scale features over the United States were an anomalously strong ridge over much of the country, with a smaller-scale slow-moving circulation located equatorward of the ridge (Figs. 1a and 1b). Rainfall during this 5-day period, which exceeded 300 mm in much of southeastern Kansas, caused deadly and destructive flooding: four fatalities and $350M in damage were reported (NOAA 2007). Some of the most serious impacts occurred in Coffeyville, Kansas, where an oil spill was caused when floodwaters overtopped a levee and infiltrated a refinery (NOAA 2007).

In addition to these impacts, this event is of interest because, in relation to other heavy rain events of similar spatial and temporal scales, medium-range forecasts of this event had low skill and large uncertainty (Schumacher and Davis 2010). Other warm-season heavy rainfall events in the southern United States have also been found to have limited predictability (e.g., Nielsen-Gammon et al. 2005; Zhang et al. 2006). As such, an investigation of the atmospheric processes that were associated with the relatively poor medium-range

* Supplemental information related to this paper is available at the Journals Online Web site: http://dx.doi.org/10.1175/MWR-D-10-05022.s1.

Corresponding author address: Russ Schumacher, Dept. of Atmospheric Sciences, Texas A&M University, College Station, TX 77843.
E-mail: russ.schumacher@tamu.edu

DOI: 10.1175/MWR-D-10-05022.1

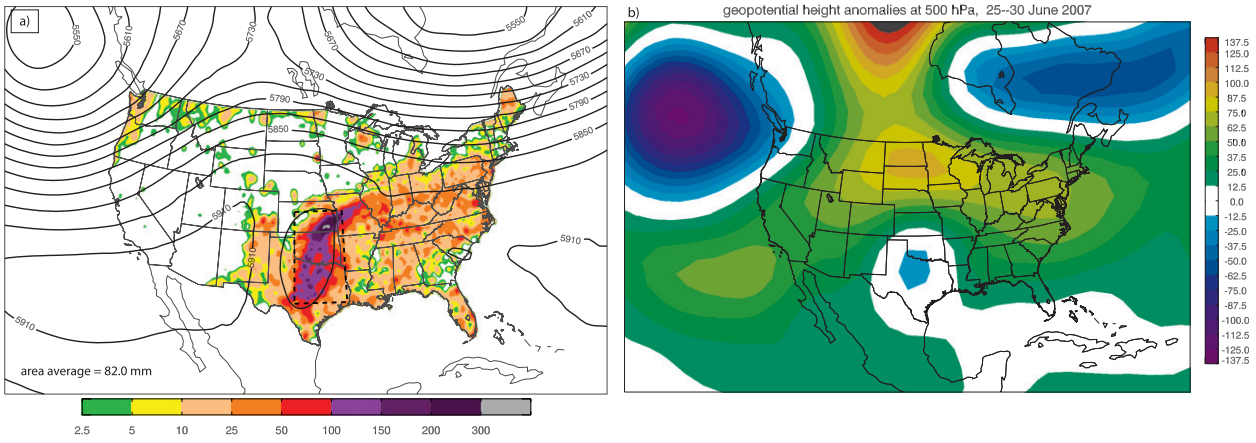

FIG. 1. (a) Climate Prediction Center (CPC) unified gauge-based precipitation analysis (color shading in mm; Chen et al. 2008) for the 120-h period 1200 UTC 25 Jun–1200 UTC 30 Jun 2007 and average 500-hPa geopotential height (contoured every 30 m) from 12-hourly ECMWF deterministic model initializations over the same time period. The dashed black rectangle indicates the location for areal averaging of precipitation and other fields. (b) National Centers for Environmental Prediction–National Center for Atmospheric Research (NCEP–NCAR) reanalysis (Kalnay et al. 1996) 500-hPa geopotential height anomaly for 25–30 Jun 2007, relative to the 1968–96 mean.

forecasts in this case is warranted. Further, the availability of large global ensemble datasets, such as the The Observing System Research and Predictability Experiment (THORPEX) Interactive Grand Global Ensemble (TIGGE; Bougeault et al. 2010), allows for quantitative analysis of synoptic- and mesoscale factors associated with the development or nondevelopment of widespread heavy precipitation. One purpose of this study is to evaluate the utility of the TIGGE dataset for this sort of meteorological diagnosis.

b. *Use of ensembles for investigating weather systems*

As ensembles of numerical weather prediction models have gained greater use in weather forecasting and techniques for ensemble data assimilation have been developed, some investigators have used ensemble forecasts to gain quantitative insights into the dynamics of weather systems. Hakim and Torn (2008) summarized these techniques in an analysis of a midlatitude cyclone, and Torn (2010) applied the techniques to examine the dynamics of the extratropical transition of tropical cyclones (TCs). Similar techniques were used by Hawblitzel et al. (2007), Sippel and Zhang (2008), and Sippel and Zhang (2010) to explore the genesis of mesoscale convective vortices (MCVs) and TCs. The specific uses of these techniques in the present study will be given in section 3.

These studies used numerical simulations that were designed and run to examine specific cases of interest. In contrast, the present study will use archived operational ensemble forecasts. The primary benefit of using operational forecasts is that they are readily available and represent the modeling systems currently used for weather forecasting (and, thus, the forecast skill and uncertainty that a forecaster would be presented with). They also allow for the possibility of studying numerous cases with minimal additional computational investment. A substantial downside to using operational forecasts is that it is not possible to run sensitivity tests or otherwise experiment with these forecasts; the data are static. Further possible limitations of using the operational forecasts will be discussed in sections 3 and 5.

c. *Genesis of warm-core vortices*

A topic of much interest in the recent scientific literature is the process by which warm-core vortices, such as TCs and MCVs, develop and intensify. In particular, discerning the factors that determine which vortices will strengthen and which will not is important to both scientific understanding and operational forecasting. As will be demonstrated in the analysis in this manuscript, the heavy rainfall during 25–30 June 2007 was associated with a slow-moving warm-core vortex over the southern Great Plains.

For TCs, numerous studies have analyzed the large-scale factors that contribute to or detract from genesis (e.g., Gray 1968; McBride and Zehr 1981; Hennon and Hobgood 2003, Schumacher et al. 2009; Kerns and Zipser 2009). Factors that have been suggested as important discriminators between developing and nondeveloping vortices include strong low-level vorticity and convergence around the incipient vortex, weak vertical wind shear, and increased midlevel moisture and conditional instability. Similarly, Trier et al. (2000)

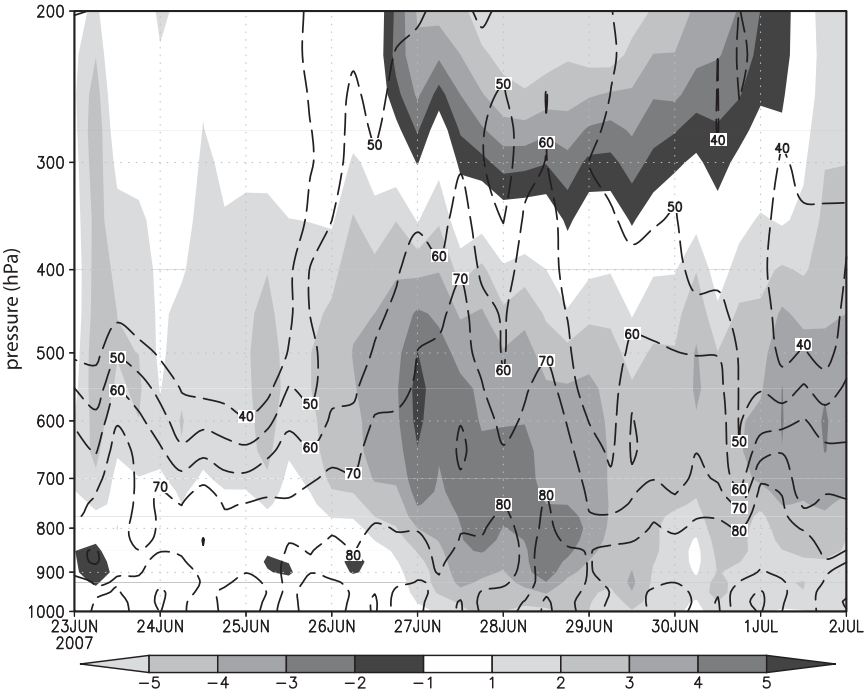

FIG. 2. Time–height diagram from 23 Jun to 2 Jul 2007 of relative vorticity (10^{-5} s^{-1}, shaded) and RH (dashed contours every 10% starting at 40) from the 3-hourly North American Regional Reanalysis (Mesinger et al. 2006). Values are averaged over the rectangle shown in Fig. 1.

found that convection near continental MCVs on subsequent days was favored with stronger vortices, when the vertical wind shear was relatively weak, and the environment surrounding the MCV was moist and unstable. This secondary convection is necessary for maintaining an MCV beyond a single diurnal cycle (Bosart and Sanders 1981; Fritsch et al. 1994) and also creates the possibility for development of a low pressure center at the surface (e.g., Hawblitzel et al. 2007; Schumacher and Johnson 2008; James and Johnson 2010).

In the present study, these and other factors will be examined in medium-range ensemble forecasts of the 25–30 June 2007 rain event to find the reasons why some ensemble members produced a long-lived, slow-moving vortex with associated heavy rainfall, and others did not. Section 2 will provide an overview of the event, and section 3 will describe the data and methods used in the study. In section 4, results of the ensemble-based analysis will be presented, section 5 will contain a discussion, and section 6 will conclude the manuscript.

2. Event overview

The widespread heavy rainfall over the southern plains in late June 2007 began with an area of midlevel cyclonic vorticity that became centered closer to the surface over time (Fig. 2). As noted by Goebbert et al. (2008), an initial MCV developed in Texas on 22 June that then dissipated, though some weak vorticity remained in the area. Another small MCV developed in association with convection on 23–24 June (Goebbert et al. 2008). A few small, weakly organized mesoscale convective systems (MCSs) formed over Texas during the day on 24 June 2007, with convection remaining near the MCV early on 25 June (Fig. 3a). During the afternoon of 25 June, more widespread convection developed across Texas, with a convective line moving northward from the Gulf of Mexico coast through east Texas, and slower-moving convection persisting into the night in central Texas (see the online supplement to this paper for animated radar imagery). A broad, closed midlevel circulation had developed by 0000 UTC 26 June (Fig. 4b), but there was not a low-level circulation in this area at this time (Figs. 4a and 2). A large MCS formed in southern Oklahoma around 0900 UTC 26 June, which moved southward and persisted through the day, while a large area of weaker convection moved northward on the east side of the midlevel vorticity maximum (Fig. 3b). By 0000 UTC 27 June, a broad circulation—much larger in horizontal scale than the original MCV—was apparent in animations of radar imagery, and this corresponded to a maximum in both mid- and low-level vorticity (Figs. 4c,d and 2). This circulation was associated with deep moisture, strong

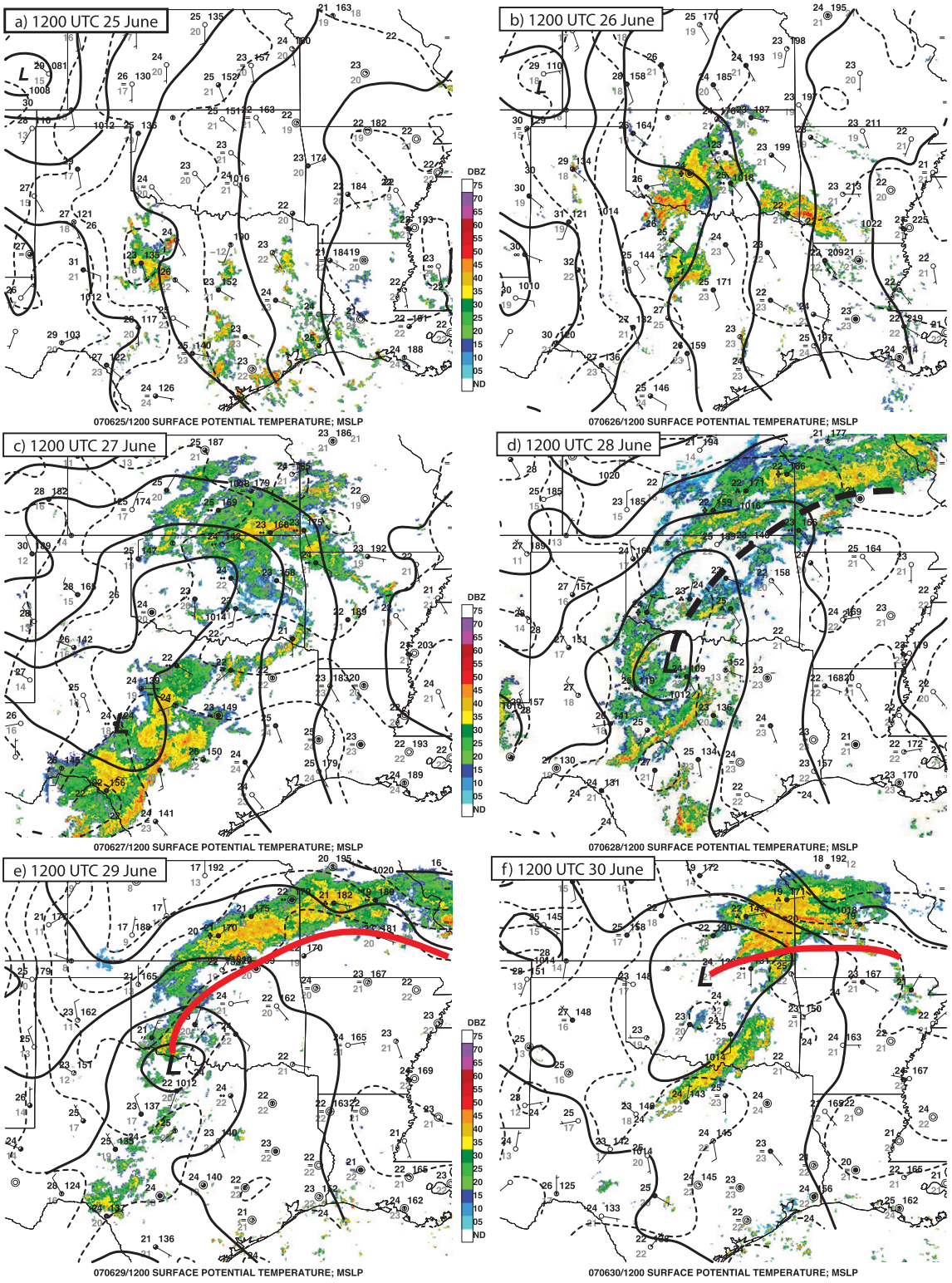

FIG. 3. Barnes objective surface analysis (Koch et al. 1983) showing pressure adjusted to sea level (solid contours every 2 hPa), surface potential temperature (gray dashed contours every 2°C), and station model [conventional, with temperature (°C) and sea level pressure in black and dewpoint (°C) in gray]. Also shown is composite radar reflectivity from the WSI Corporation's NOWrad product. Times shown are 1200 UTC on (a) 25, (b) 26, (c) 27, (d) 28, (e) 29, and (f) 30 Jun 2007. The location of a pressure trough is shown by the thick dashed line in (d), the location of a warm front is shown by the red lines in (e) and (f).

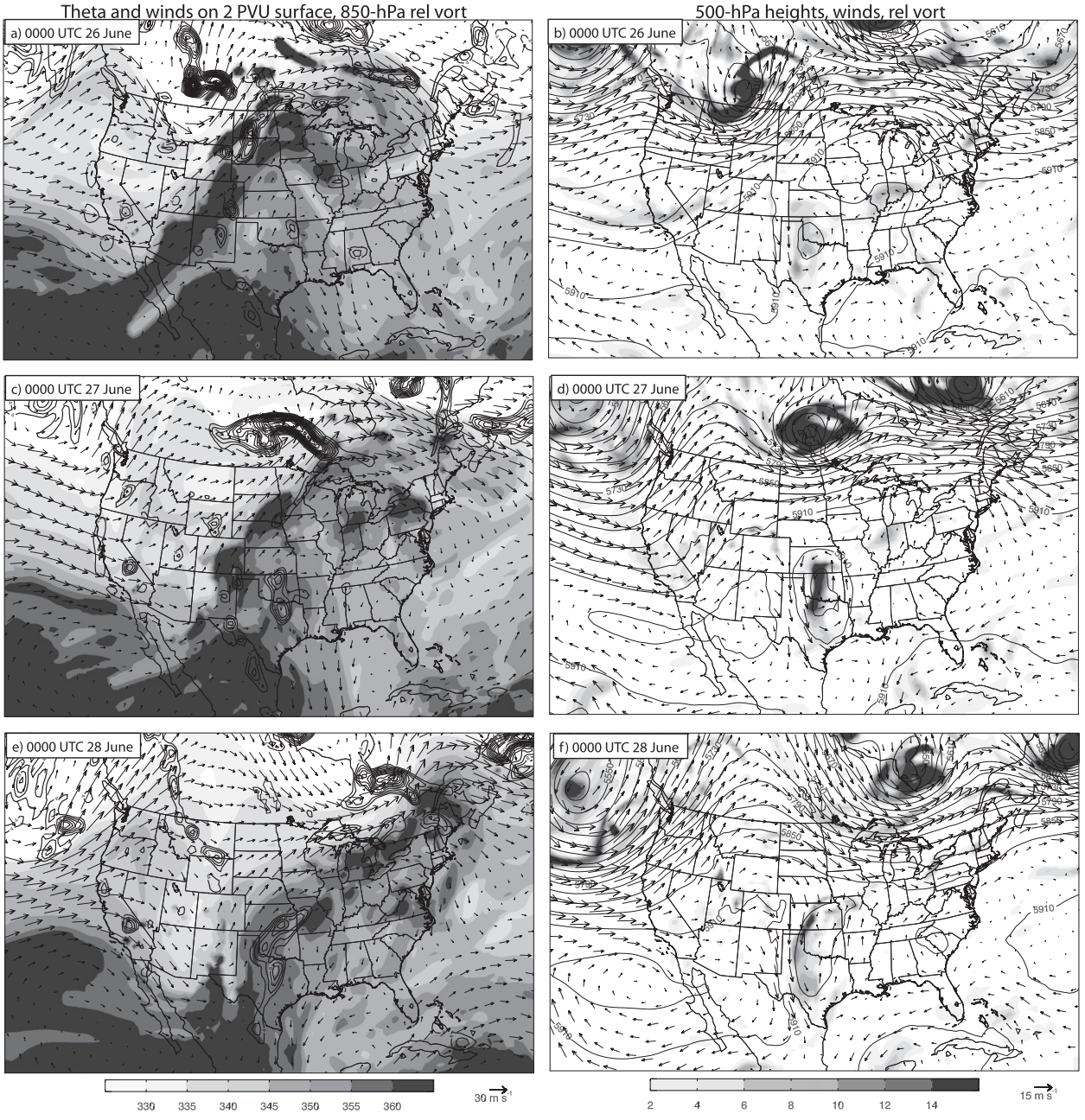

FIG. 4. (a),(c),(e) Potential temperature (K, shaded) and winds (m s^{-1}) on the dynamic tropopause and 850-hPa relative vorticity (positive values contoured every 2×10^{-5} s^{-1} starting at 4) from ECMWF deterministic model initializations at (a) 0000 UTC 26 Jun, (b) 0000 UTC 27 Jun, and (c) 0000 UTC 28 Jun 2007. The dynamic tropopause is defined here as the 2-PVU surface, where 1 PVU = 10^{-6} m^2 s^{-1} K kg^{-1}. (b),(d),(f) The 500-hPa geopotential height (contoured every 30 m), relative vorticity (10^{-5} s^{-1}, shaded), and wind vectors from ECMWF deterministic model initializations at (b) 0000 UTC 26 Jun, (d) 0000 UTC 27 Jun, and (f) 0000 UTC 28 Jun 2007.

anticyclonic upper-level outflow, and ridging on the dynamic tropopause, characteristic of a warm-core cyclone (Figs. 2 and 4b). On 27 June 2007, several large MCSs developed (Fig. 3c): one moving southward through central Texas during the afternoon, a large squall line propagating eastward from the high terrain of New Mexico, and a weaker northward-moving MCS in Oklahoma. As these MCSs matured and then dissipated, the large-scale vorticity maximum became centered nearer the ground (Fig. 2) and two closed surface low pressure centers developed: one in south-central Texas and one in southwestern Oklahoma (Fig. 3c). These

surface lows eventually merged on 28 June (Fig. 3d), and convection continued surrounding this cyclone. The most persistent rainfall occurred poleward of the surface low along a warm front in southeastern Kansas and western Missouri (Fig. 3e). The front was partly the remnant of the cold front of a midlatitude cyclone that moved eastward across southern Canada on 26–27 June (Figs. 4a, 4c, and 4e). This convection persisted in a similar manner through 29–30 June (Fig. 3f), with the coverage and intensity of the convection weakening somewhat on 1 July. Over the 5 days of the event, rainfall amounts exceeded 100 mm over large parts of Texas, Oklahoma, Kansas, and Missouri, with southeastern Kansas receiving over 300 mm (Fig. 1). This rainfall contributed to record-breaking seasonal and annual rainfall totals in the plains (Goebbert et al. 2008).

3. Data and methods

The remainder of the study will use ensemble forecasts as an analysis tool to determine the synoptic- and mesoscale factors that led to the development of the vortex and its associated heavy rainfall. The primary ensemble forecast that will be used is the European Centre for Medium-Range Weather Forecasts (ECMWF) Ensemble Prediction System (Buizza et al. 2007) forecast initialized at 0000 UTC 24 June 2007. It is a 51-member ensemble with a spectral truncation of T399 (corresponding to approximately 50-km horizontal grid spacing) and 62 vertical levels through 240 forecast hours. The ensemble comprises a control run and 50 members that are initially perturbed by singular vectors in pairs (i.e., a positive and negative perturbation) and by stochastic physics (ECMWF 2010a). The singular vector perturbations have a horizontal scale of T42 with 62 vertical levels, and are designed so that their impact is maximized over Europe at 48 h into the forecast. Forecasts for all 51 members were obtained on a 0.5° latitude × 0.5° longitude grid from the TIGGE archive (information online at http://tigge-portal.ecmwf.int).

This model and initialization time were chosen for several reasons, the most important being that it included ensemble members that had very accurate forecasts of both the rainfall and the vortex, as well as members with very little precipitation over the southern plains (Fig. 5). Although none of the ensemble members predicted as much rain as was observed, a few members (e.g., Figs. 5a and 5c) realistically reflected the spatial distribution of precipitation and the evolution of the vortex. The ensemble forecast from this initialization time had large spread in its precipitation forecasts [see Fig. 7 of Schumacher and Davis (2010), it is the 36–168-h forecast shown there] and represented a balance between shorter-lead forecasts that had smaller spread, and longer-lead forecasts where no ensemble members had an accurate prediction of the heavy rainfall. This wide range of possible outcomes allows for an analysis of the factors that were conducive to, or detracted from, the development of the vortex-related rainfall. In general, the ECMWF ensemble has also been shown to be generally well tuned, with ensemble spread similar to the root-mean-square error of the ensemble mean (Park et al. 2008). Ensemble forecasts from other centers were also considered, but did not have the combination of spread, number of ensemble members, and members with accurate forecasts that the ECMWF ensemble did for this case.

As mentioned above, other reasons for selecting an operational ensemble for this research are that it represents what an operational forecaster might have used as guidance in advance of the event and that the data are readily available via TIGGE. There are also some disadvantages to using operational forecasts. First, the data are fixed and thus do not lend themselves to further experimentation, and only certain variables and atmospheric levels are available. Second, the initial perturbations are on large spatial scales (T42), and thus do not include mesoscale uncertainties that may be important to an event such as this in which mesoscale convection likely plays an important role. Third, the resolution of the model does not allow for explicitly predicted convection; instead, the convection is parameterized. However, there is not currently an operational medium-range forecast model that has sufficient resolution for explicit convection. Thus, individual organized convective systems will not be predicted explicitly (and will not be a focus of the analysis). Finally, although the ensemble is designed to represent a range of possible outcomes, the perturbed initial conditions in the ensemble members do not necessarily represent equally likely estimates of the initial state (e.g., Hakim and Torn 2008). To partially overcome the third and fourth limitations, the analysis in the present study will use an area-averaged dependent variable, and will examine only fields from at or beyond 36 h into the forecast, such that the ''memory'' of the initial perturbations is reduced, the model atmosphere has come into balance in each of the ensemble members, and it can be more safely assumed that each member is representing an equally likely outcome.

In particular, the dependent variable used throughout the study is the forecast 36–156-h accumulated precipitation, areally averaged over the southern plains (hereafter abbreviated *P*; averaging box shown in Fig. 1). This allows for an investigation of the important factors in the event as a whole, rather than that of any specific

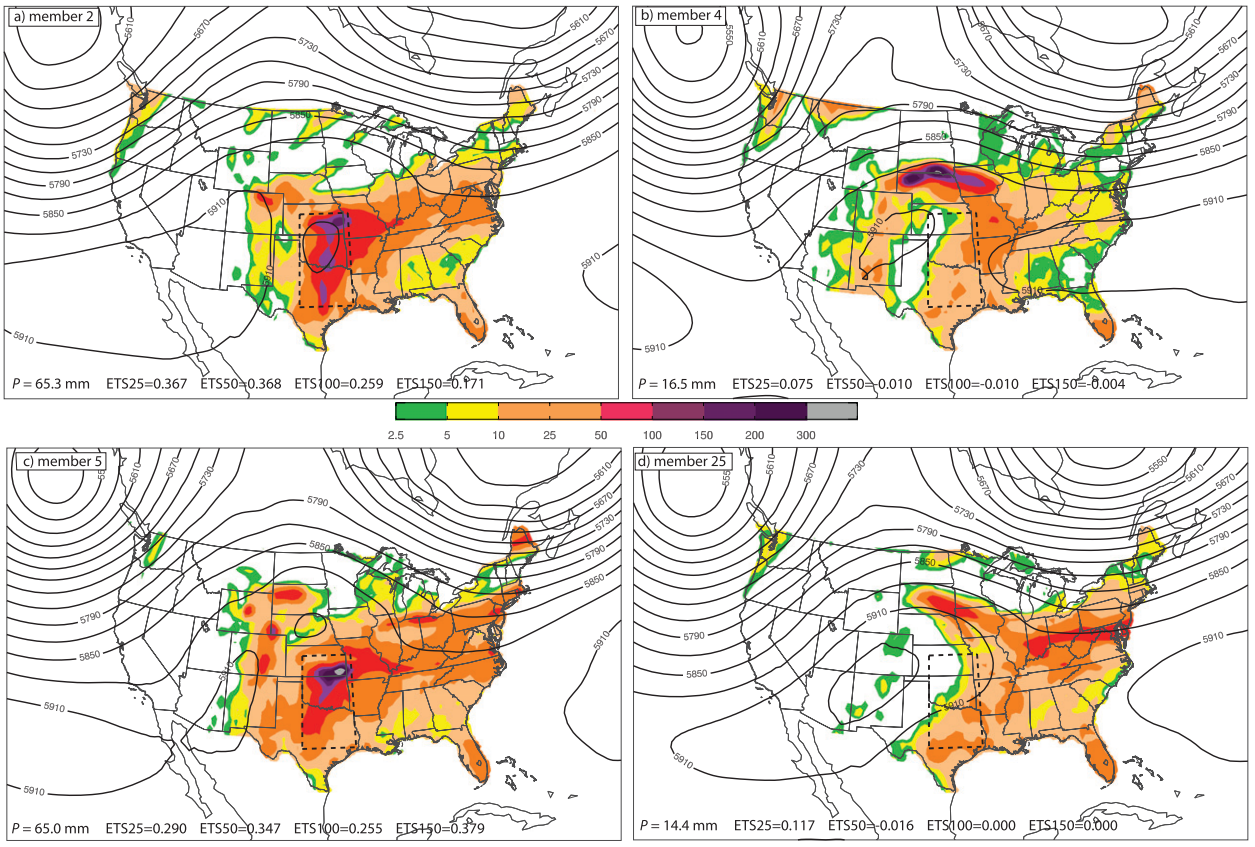

FIG. 5. As in Fig. 1a, but for example ECMWF ensemble members initialized at 0000 UTC 24 Jun 2007. Shown are ensemble members (a) 2, (b) 4, (c) 5, and (d) 25, representing the (a),(c) best and (b),(d) worst of the members in terms of precipitation forecasts. Precipitation outside the United States has been masked out for visual comparison with the observations in Fig. 1. The value of P, the 36–156-h precipitation forecast averaged over the area within the dashed rectangle, is shown in the bottom left of each panel. Furthermore, values of equitable threat score [ETS, calculated using Eq. (17) of Hamill and Juras (2006)] over the entire United States at different precipitation thresholds are shown (e.g., ETS25 is the ETS at the 25-mm threshold). The best and worst forecasts shown here are those with the highest and lowest predicted values of P.

rainfall maximum. Among the ensemble members, this varies from a minimum of 14.4 mm in member 25 (Fig. 5d) to a maximum of 65.3 mm in member 2 (Fig. 5a), compared with the observed value of 82 mm (Fig. 1). Following the approach used in, for example, Sippel and Zhang [(2008), their Eq. (3)], linear correlations between several atmospheric variables and P within the ensemble are calculated at each grid point and forecast time. Assuming that beyond forecast hour 36 the 51 ensemble members are equally likely, correlations with magnitudes greater than approximately 0.36 are statistically different from zero at the 99% confidence level using a two-tailed significance test. Although not implying causation, the correlation between variables shows the presence of linear relationships that can be used in tandem with physical interpretation to understand the behavior of the ensemble forecasts. Also, as in Sippel and Zhang (2008), Hakim and Torn (2008), and others, linear statistics are used here for simplicity, with the recognition that there may be nonlinear relationships that are neglected as a result.

Covariance between atmospheric variables and P is also calculated as in Hakim and Torn [(2008), their Eq. (14)], normalized by the standard deviation of P in the ensemble (12.0 mm) so that the resulting values are in the physical units of the independent variable. Together, the correlation and covariance analyses provide information about the strength of the linear relationship between P and other variables, with the covariance representing the slope of the line and the correlation representing how well that line approximates the relationship. In the following section, correlation and covariance maps will be presented and discussed, first to demonstrate that the ensemble forecasts represent physically reasonable outcomes, and second to elucidate the processes that were favorable or detrimental to the development of widespread heavy rain in this case.

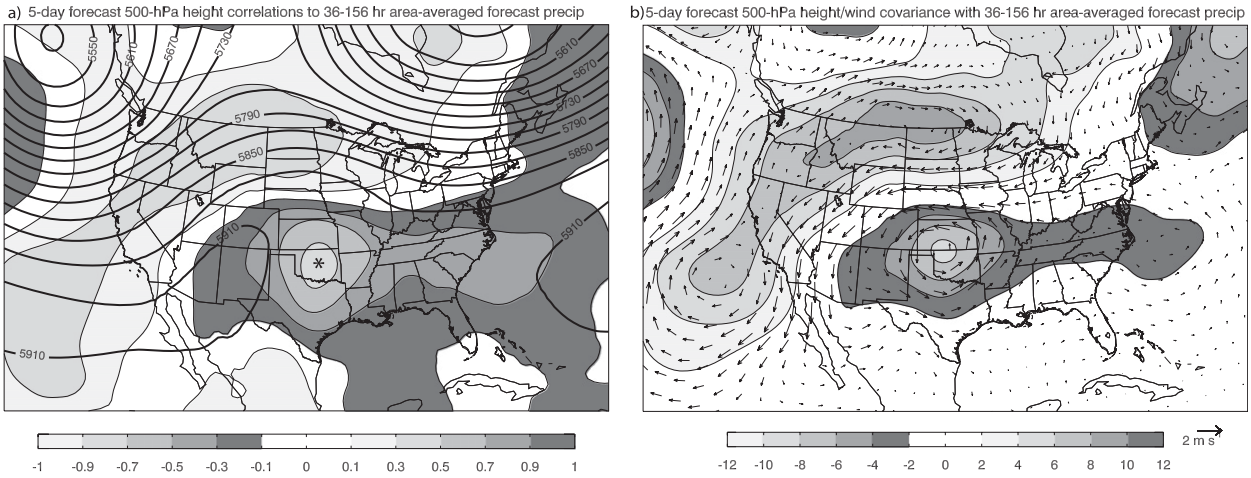

FIG. 6. (a) Correlation of time-averaged 36–156-h forecast 500-hPa height (valid from 1200 UTC 25 Jun to 1200 UTC 30 Jun 2007) with *P* (shaded), and ensemble-mean 36–156-h forecast 500-hPa height (contoured every 30 m). (b) Covariance of time-averaged 36–156-h forecast 500-hPa height (m, shaded) and wind (vectors) with *P*, normalized by the standard deviation of *P*. The asterisk in (a) shows the location used for the scatterplot in Fig. 7.

4. Results

a. 5-day-average midtropospheric pattern

Before examining the precursors to the development or nondevelopment of heavy rainfall in the ensemble, temporally averaged 36–156-h forecast 500-hPa fields are examined to illustrate the overall behavior of the ensemble at the synoptic scale and its relationship to precipitation in the southern plains. The ensemble mean height pattern is broadly similar to the analysis over this 5-day period, with a ridge over the central United States and troughs in the Gulf of Alaska and northeastern Canada (cf. Figs. 6a and 1a). There are strong negative correlations ($r \leq -0.7$) between the 5-day forecast 500-hPa height and *P* over the southern plains (Fig. 6a). This is consistent with the idea that the maintenance of a long-lived vortex over Oklahoma was closely linked to the occurrence of widespread heavy rainfall there, as the ensemble members with lower heights over the southern plains also had significantly more precipitation in that area. There are weaker positive correlations between 500-hPa height and *P* extending southwestward from the northern plains into the Pacific Northwest and the eastern Pacific (Fig. 6a).

A height covariance map shows signals in similar places, with magnitudes of 3–9 m at 500 hPa per standard deviation change in *P* (Fig. 6b). Wind covariance suggests that these are balanced, coherent features in the ensemble, further demonstrating the relationship between a midlevel vortex and the heavy rainfall (Fig. 6b). These statistics can be summarized in a scatterplot relating the forecast 500-hPa height at a point in central Oklahoma to *P* (Fig. 7). It shows a strong linear relationship between these two variables, with higher (lower) heights corresponding to less (more) precipitation. Of course, the mass and wind fields at 500 hPa are also strongly correlated with other atmospheric variables, so this is not meant to suggest that 500-hPa height could be used as a ''predictor'' of rainfall (nor is rainfall a predictor of 500-hPa height) in any sense. But the 500-hPa height represents one measure of the strength

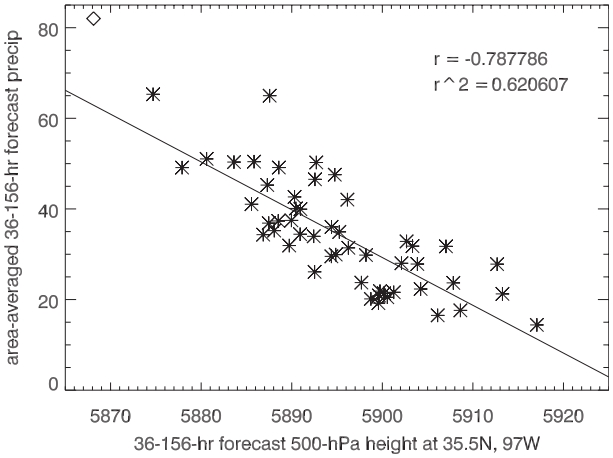

FIG. 7. Scatterplot of the 51 ensemble members (indicated by asterisks), with forecast 36–156-h 500-hPa height at a point in central OK (35.5°N, 97°W; location shown in Fig. 6a) along the abscissa and *P* along the ordinate. The correlation coefficient and its square are given in the top right, and the observed values are shown by the diamond. The linear least squares fit line is also shown.

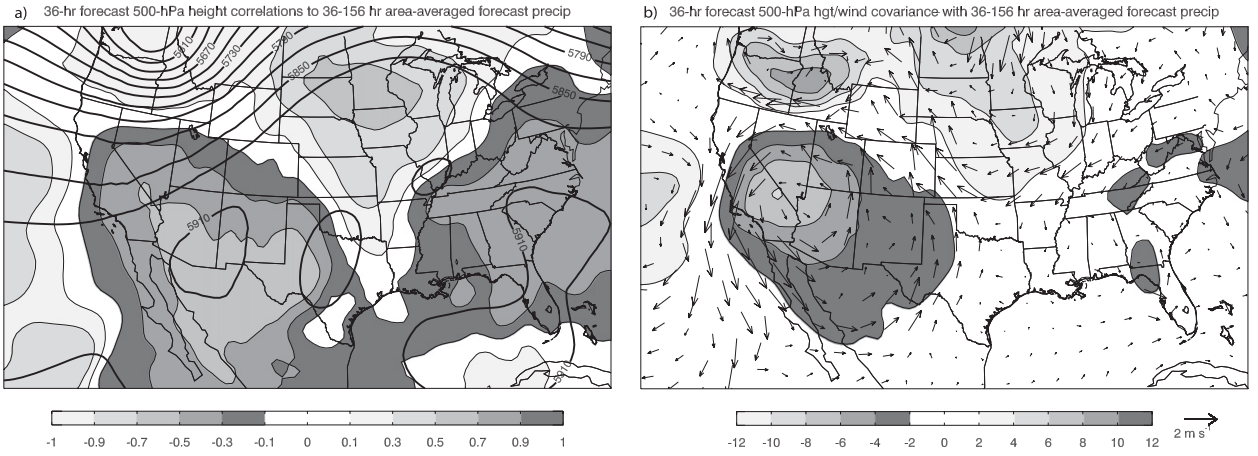

FIG. 8. As in Fig. 6, but for instantaneous correlations and covariance with *P* at forecast hour 36 (1200 UTC 25 Jun 2007).

of the southern plains vortex, and these data point to a strong relationship between the presence (and strength) of a vortex and the total precipitation there. The observed height and precipitation are also consistent with this linear relationship, although all of the ensemble members underpredicted the total precipitation and the overall strength of the midlevel vortex (Fig. 7). One possible reason for the underprediction is the relatively coarse spatial resolution of the ECMWF ensemble in comparison with the scale of observed precipitation systems.

Now that the temporally averaged characteristics of the ensemble have been established, the relationships discussed above will be examined more closely to show how they evolved over time and space. It is not a particularly surprising result that a stronger vortex would be associated with more rainfall; perhaps the more interesting question is what factors were supportive of, or detracted from, the development and maintenance of the vortex? Statistical analysis of the ensemble will be used to explore this question and to relate the results to physical mechanisms that may have supported or inhibited the development of the vortex and its associated rainfall.

b. Large-scale factors influencing the development of the vortex and heavy rainfall

1) CORRELATIONS AND COVARIANCE

Figure 2 shows that the area-averaged midlevel cyclonic vorticity, as well as the anticyclonic outflow aloft, intensified at approximately 0000 UTC 27 June, or hour 72 in the forecast ensemble used here. As a result, forecast atmospheric fields leading up to this time can be considered as precursors to the development of the warm-core vortex over the southern plains, and correlations and covariance of these fields with *P* will be examined in this section. During this time period, some of the strongest correlations with *P* are found in the 500-hPa height field (Fig. 8a). At 1200 UTC 25 June (forecast hour 36), two areas have large areas with correlation magnitudes greater than 0.5: negative correlations over the southwestern United States and northern Mexico, and positive correlations over the northern plains and Midwest (Fig. 8a). These are associated with an ensemble-mean anticyclone to the west and a ridge to the north of the incipient vortex, respectively, and suggest that a weaker southwest anticyclone and a stronger Midwest ridge at this time were associated with greater precipitation in the southern plains during the subsequent 5 days.

The 500-hPa height covariance with *P* at this time is relatively small over this area, however (Fig. 8b), with the strongest signals appearing closer to the trough over the west coast of the United States where the ensemble spread was greater at this time (not shown). This suggests that although the magnitude of the differences in 500-hPa height in west Texas, southern New Mexico and Arizona, and northern Mexico between members with more precipitation and those with less may be small, there is a robust relationship. Similar structures are apparent at 250 hPa (not shown), only they are shifted somewhat to the west and the correlations with *P* are weaker.

There are also correlations between the wind fields at hour 36 and *P*. East of the Rocky Mountains, there is a large area where the 500-hPa meridional wind has a correlation coefficient >0.5 with *P* (Fig. 9a). The ensemble mean wind in this area is weak, with northerly flow over western Texas and northern Mexico. This suggests that either weakened northerly winds or an enhanced southerly component to the wind was associated with greater *P*. With mean southerly winds at low

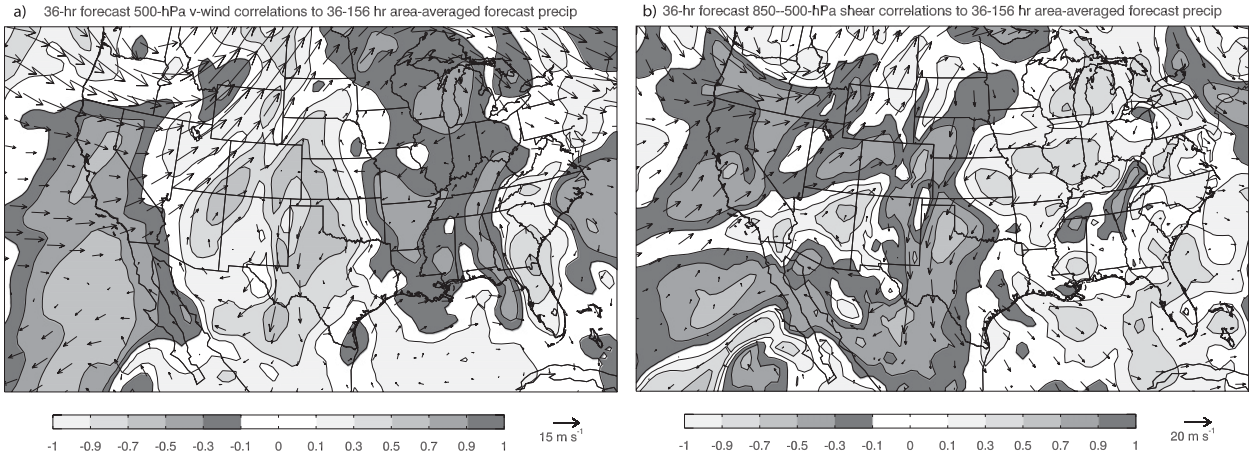

FIG. 9. (a) Correlation of 36-h forecast 500-hPa meridional wind (valid 1200 UTC 25 Jun 2007) with P (shaded) and 36-h forecast ensemble-mean 500-hPa wind vectors. (b) As in (a), but for 850–500-hPa vector shear magnitude and 850–500-hPa shear vectors.

levels at this time (not shown), and considering the generally accepted idea that weaker vertical shear of the horizontal wind is more favorable for the development and maintenance of warm-core vortices (e.g., Trier et al. 2000), it is possible that the ensemble members with stronger vertical shear may have been less likely to develop a long-lived vortex over the southern Great Plains. In fact, the magnitude of the 850–500-hPa shear is generally negatively correlated with P over the southern plains at forecast hour 36 (Fig. 9b), a relationship that continues and becomes more robust through hour 60 (Figs. 10a and 10b).

When averaged over the southern plains (using the same averaging area as that used to calculate P), the magnitude of the 850–500-hPa wind shear at hour 60 was strongly anticorrelated with P ($r = -0.75$; Fig. 11). Thus, it appears that one of the key factors distinguishing ensemble members that developed a long-lived, widespread rain event from those that did not was the magnitude of the northerly wind shear over the incipient vortex, with weaker northerly shear being associated with a stronger vortex and more rainfall at later times. This is also consistent with the anticorrelation between 500-hPa height and P in the southwestern United States (Fig. 8a), where a weaker anticyclone in the southwest was associated with weaker northerly midlevel winds over the incipient vortex. The physical interpretation of these results will be explored more thoroughly in the next subsection.

Three other items of concern for forecasting this event are apparent from Fig. 11. First is that, as mentioned previously, the observed area-average precipitation lies well outside of the envelope predicted by the ensemble (i.e., although some correctly predicted the spatial distribution, all members underpredicted the total rainfall amount). As mentioned above, this may be partially

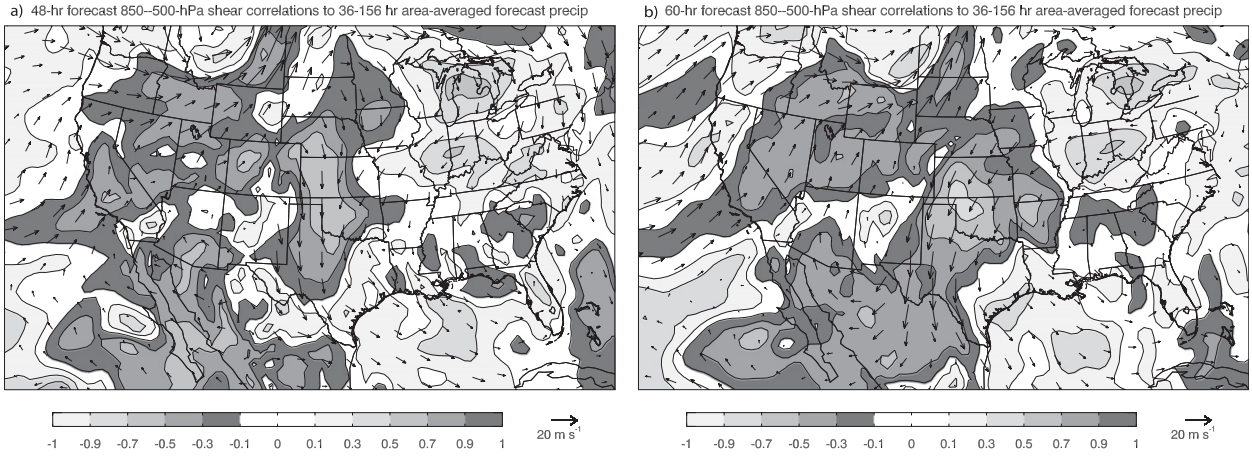

FIG. 10. As in Fig. 9b, but for forecast hours (a) 48 (valid 0000 UTC 26 Jun) and (b) 60 (valid 1200 UTC 26 Jun).

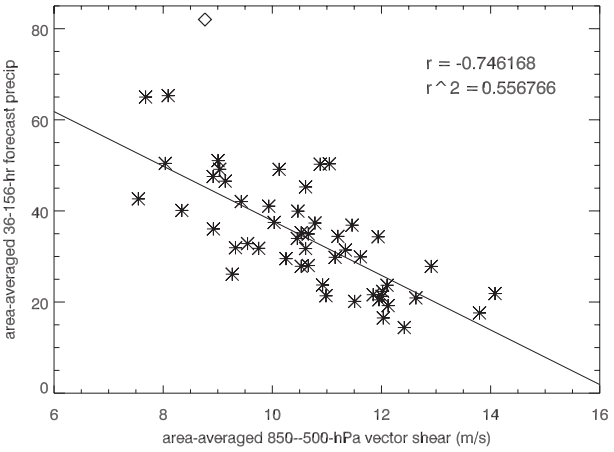

FIG. 11. Scatterplot of the 51 ensemble members (indicated by asterisks) with 60-h forecast 850–500-hPa vector shear magnitude, averaged over the area shown in Fig. 1 along the abscissa and *P* along the ordinate. The correlation coefficient and its square are given in the top right, and the observed values are shown by the diamond. The linear least squares fit line is also shown.

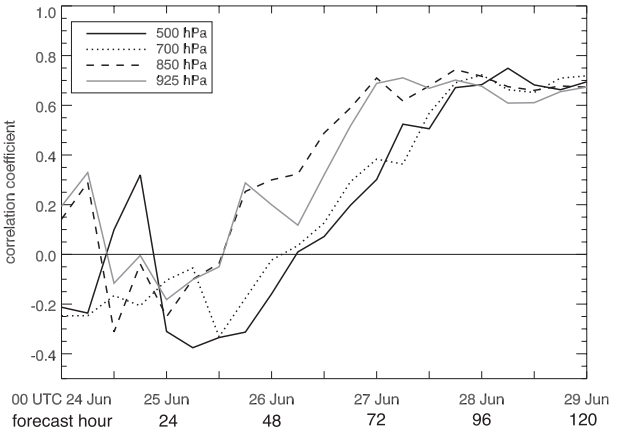

FIG. 12. Time series showing the correlations between area-averaged relative vorticity (averaged over the area shown in Fig. 5) at the 925-, 850-, 700-, and 500-hPa levels and *P*.

attributable to the spatial resolution of the model. Second is the relatively narrow range of shear magnitudes that led to widely different precipitation amounts; only a few meters per second of vertical vector shear separated the wet ensemble members from the dry ones. This suggests that relatively small short-range forecast errors in the tropospheric mass and wind fields may lead to very large errors in the medium-range precipitation forecast over a large region in a situation such as this. This chaotic pattern of behavior may be part of the reason for the poor predictions of this event in relation to other rainfall events of similar scale (Schumacher and Davis 2010). Third, at the highest values of shear predicted by the ensemble, all of the members produced very little precipitation (and a nonexistent vortex over the southern plains), which is somewhat similar to past findings regarding the development of TCs. For example, Bracken and Bosart (2000) found that the mean shear over developing tropical depressions was about 10 m s^{-1}, whereas Kerns and Zipser (2009) found that very few developing Atlantic TCs have 850–200-hPa shear magnitudes greater than 10 m s^{-1}. (The layer over which the shear is calculated is shallower in the present study than that typically used in the tropics; an anticorrelation was also found between 850–200-hPa shear and *P*, but it was not as strong as that for the 850–500-hPa shear.) Thus, as with TCs, it may be that continental warm-core vortices tend not to form under the influence of strong vertical wind shear. On the other hand, also similar to Kerns and Zipser (2009), there were several ensemble members where the shear was relatively weak, yet an intense vortex and excessive rainfall did not occur (Fig. 11). The distinctions between these members will be analyzed further in section 4c. These results are not meant to suggest that the relationship between shear and development is strictly linear; as pointed out by Bracken and Bosart (2000), some shear is necessary for TC genesis, as it fosters large-scale ascent, but too much shear can be detrimental to development. Instead, the linear correlation reveals that, within the ensemble's range of large-scale environments for this case (all of which contain some shear), there is a general inverse relationship between shear and development.

Another variable that one might expect to be correlated with *P* is the *intensity* of the vortex at earlier times; in other words, if the vortex in an ensemble member was strong early in the forecast, it may remain strong throughout the forecast. However, this does not appear to be the case, as there is little correlation between area-averaged relative vorticity and *P* prior to forecast hour 36 (Fig. 12). Only after about forecast hour 42 (1800 UTC 25 June) do consistent positive correlations between vorticity and *P* appear at low levels. Strong correlations between midlevel relative vorticity and *P* develop even later into the forecast (Fig. 12). These results come about because there was relatively little spread in the strength of the incipient midlevel vortex at early forecast times, and because coherent low-level vortices did not form in any of the members until around forecast hour 42. Similar results were also found in the correlations between horizontal deformation and *P* (not shown). The reasons why the correlations at low levels develop earlier than those at midlevels are not entirely clear, though it is possible that the members that are first to develop a strong low-level vortex are also those that are able to maintain that vortex (J. Sippel 2010, personal communication).

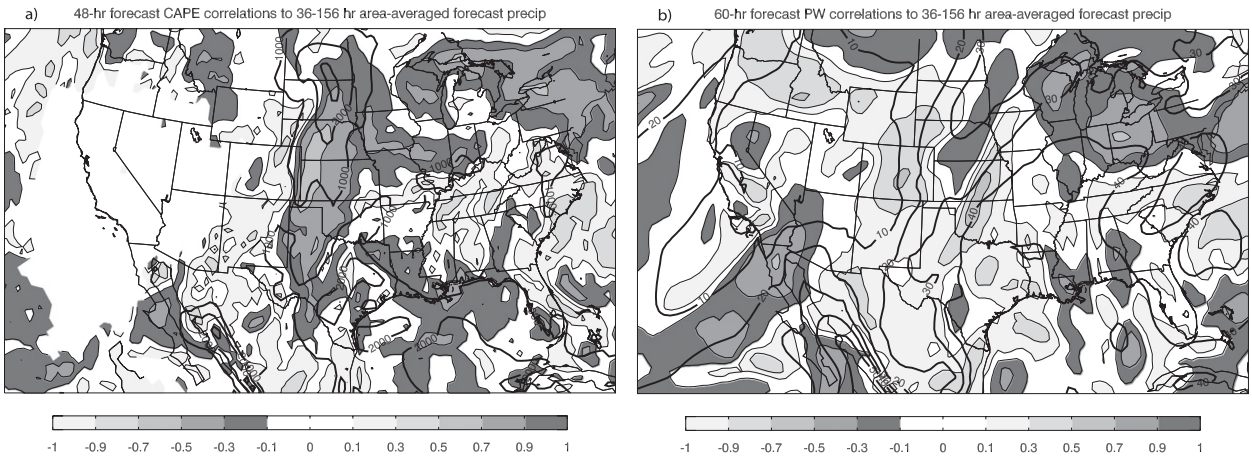

FIG. 13. As in Fig. 8a, but for correlations of (a) CAPE at forecast hour 48 and (b) TCW at forecast hour 60 with *P*. In (a), the ensemble mean CAPE is contoured every 1000 J kg^{-1} starting at 1000. In (b), the ensemble mean TCW is contoured every 10 mm starting at 10. In the ECMWF ensemble, TCW is defined as the vertical integral of (water vapor + cloud water + cloud ice) (ECMWF 2010b).

Somewhat surprisingly, correlations between variables used for diagnosing moist convection and *P* are not as strong as those seen in the synoptic-scale kinematic variables in the time leading up to the development of the warm-core vortex. One of the strongest correlations with a convective variable is actually a negative correlation between convective available potential energy (CAPE) in the Great Plains and *P* at hour 48 (0000 UTC 26 June; Fig. 13a). This represents decreased values within an axis of high CAPE that extended southward from a maximum in the Dakotas, and it is not clear whether decreased instability in this area had an effect on later convection farther southeast, or whether it was a reflection of stabilization by convection locally. The correlations between total column water (TCW) and *P* have magnitudes less than 0.5 at forecast hours 36 and 48, though a small area of $r > 0.5$ is present at hour 60 over Kansas and Oklahoma along a gradient in the ensemble mean TCW (Fig. 13b). There are a few reasons why the relationships between these variables and *P* may be relatively small. Given the large spatial scale of the initial ensemble perturbations, it is possible that variables representing atmospheric moisture are less dispersive in the ensemble than the synoptic-scale mass and wind fields. It is also possible that thermodynamics was not a strong distinguishing factor between an event and a nonevent in this case. For example, the TCW was above normal relative to climatology for this period of time, with positive TCW anomalies of 4–8 mm through most of the southern plains on 24–25 June (not shown). Thus, the thermodynamic environment was generally favorable for convection and precipitation in all ensemble members, suggesting that enhanced moisture and instability were necessary, but not sufficient, for the development of a long-lived vortex and widespread rainfall.

2) COMPOSITES

To put the previously presented results into physical perspective, composites of the six members with the highest values of *P* and the six members with the lowest values of *P* (hereafter referred to as the wet and dry members) were constructed. (Composites containing different numbers of members show similar results.) At forecast hour 36, the 500-hPa pattern is similar in both the wet and dry composites (Figs. 14a and 14b), with the incipient vortex located over the southern plains, a trough in the Pacific Northwest, and a ridge over the north-central United States. The main difference between the two composites is in the depth and location of the trough over the Pacific Northwest (Fig. 14c). However, smaller differences also exist over the southwestern United States, where the wet composite has a weaker anticyclone, and the central plains, where the wet composite has a stronger ridge (Fig. 14). The locations and signs of these differences are similar to those in the 500-hPa height correlation and covariance fields (Fig. 8).

As time progresses, the differences between the two composites increase, and the strength of the anticyclone in the southwestern United States (and its associated wind field) become particularly important. At hour 60, the incipient vortex in the wet composite is zonally broader than that in the dry composite (Figs. 15a and 15c), the anticyclone and associated flow over the southwest is weaker in the wet composite, and the shortwave trough along the California coast is also weaker in the wet composite (Fig. 15e). This is the time that was

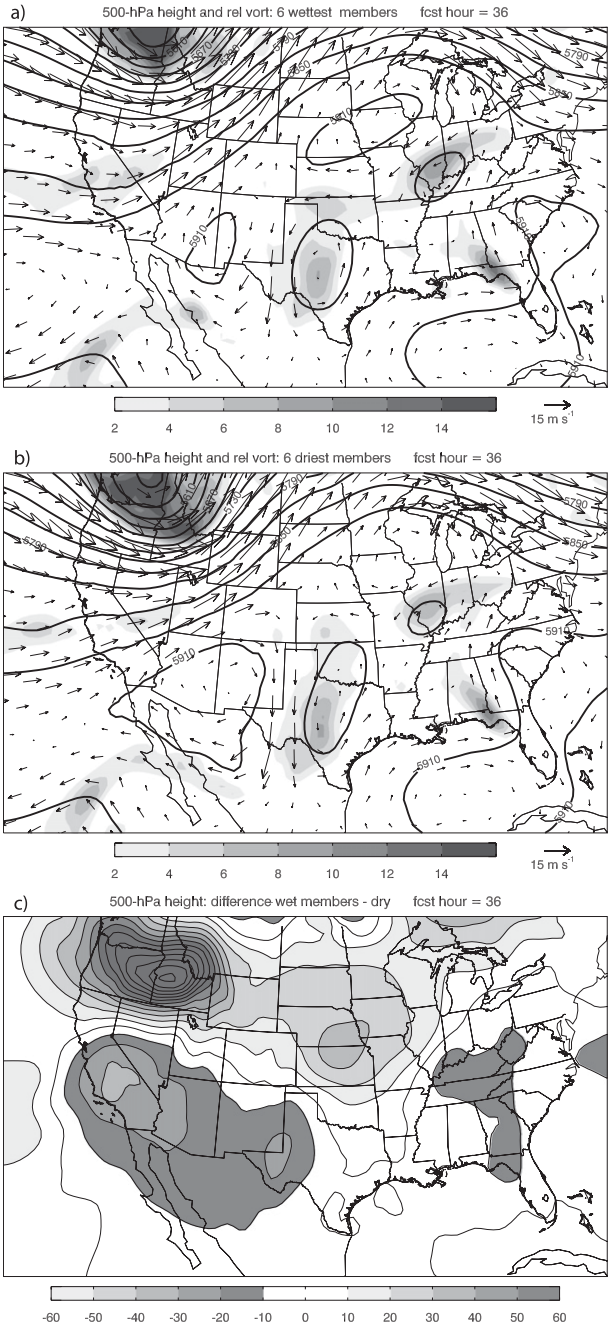

FIG. 14. The 500-hPa geopotential height (contoured every 30 m), relative vorticity (10^{-5} s^{-1}, shaded), and wind vectors at forecast hour 36 (valid 1200 UTC 25 Jun). (a) Composite of six members with the highest values of *P*, referred to as the wet composite. (b) Composite of six members with the lowest values of *P*, referred to as the dry composite. (c) Difference in 500-hPa height (m, shaded) between the wet and dry members.

shown to have very strong correlation between the 850–500-hPa vertical shear and *P* (Fig. 11), and the relevance of this shear is apparent in the composite 500-hPa winds as well; in the dry composite, there is north-northeasterly flow over western Kansas, Oklahoma, and Texas, whereas the wet composite has weaker northerly or even easterly winds in this area (Figs. 15a and 15c). In addition to these differences in the vertical wind shear, there is also less horizontal deformation taking place at midlevels over the southern plains in the wet composite (not shown explicitly, but inferred from Figs. 15a–d).

In addition to shearing the incipient vortex, the stronger northerly shear in the dry composite also results in convection occurring farther downshear (south) of the vorticity maximum (Fig. 16b), whereas the weaker shear in the wet composite allows convective precipitation to occur closer to the vorticity center (Fig. 16a). This likely results in an intensification of the midlevel vortex via latent heat release and potential vorticity redistribution (e.g., Haynes and McIntyre 1987) farther north in the wet members; whereas this process occurs farther south (and also undergoes stronger shear) in the dry members. As noted by Davis and Bosart (2004, their Fig. 3) for the genesis of TCs via the tropical transition mechanism, convection occurring upshear of the incipient low tends to be more favorable for later development, as the convection itself serves to reduce the shear over the low. The differences in the location of precipitation between the two composites appear to be related more to these kinematic influences than to thermodynamic factors, as there was an axis of high CAPE (more than 2000 J kg^{-1}) across central Texas in both composites (not shown explicitly, but shown in the ensemble mean in Fig. 13a), and differences in TCW across Texas between the composites were only a few millimeters (not shown).

By hour 72, the southwest anticyclone has strengthened further in the dry composite, as the 5940-m height contour has moved into western Kansas and southern Nebraska (Fig. 15d) and there are north-northeasterly winds across the north side of the vortex. As a result of this, and of the convection being located farther south, the cyclonic vorticity maximum has moved into southwest Texas. In the wet composite, on the other hand, the southwest anticyclone is much weaker, as are the northerly winds on the north side of the vortex, and the composite vorticity maximum has moved northward into central Oklahoma (Figs. 15b and 15f). In the wet members, this vortex then remains over the southern plains in a similar manner to what was observed, whereas the vortex in the dry members moves southwestward into the high terrain of Mexico and dissipates. Because the composites become overly smoothed at later times, owing to slightly different positions of vorticity maxima among the ensemble members included in the composites, the composites are not shown at these later times. However, two representative ensemble members

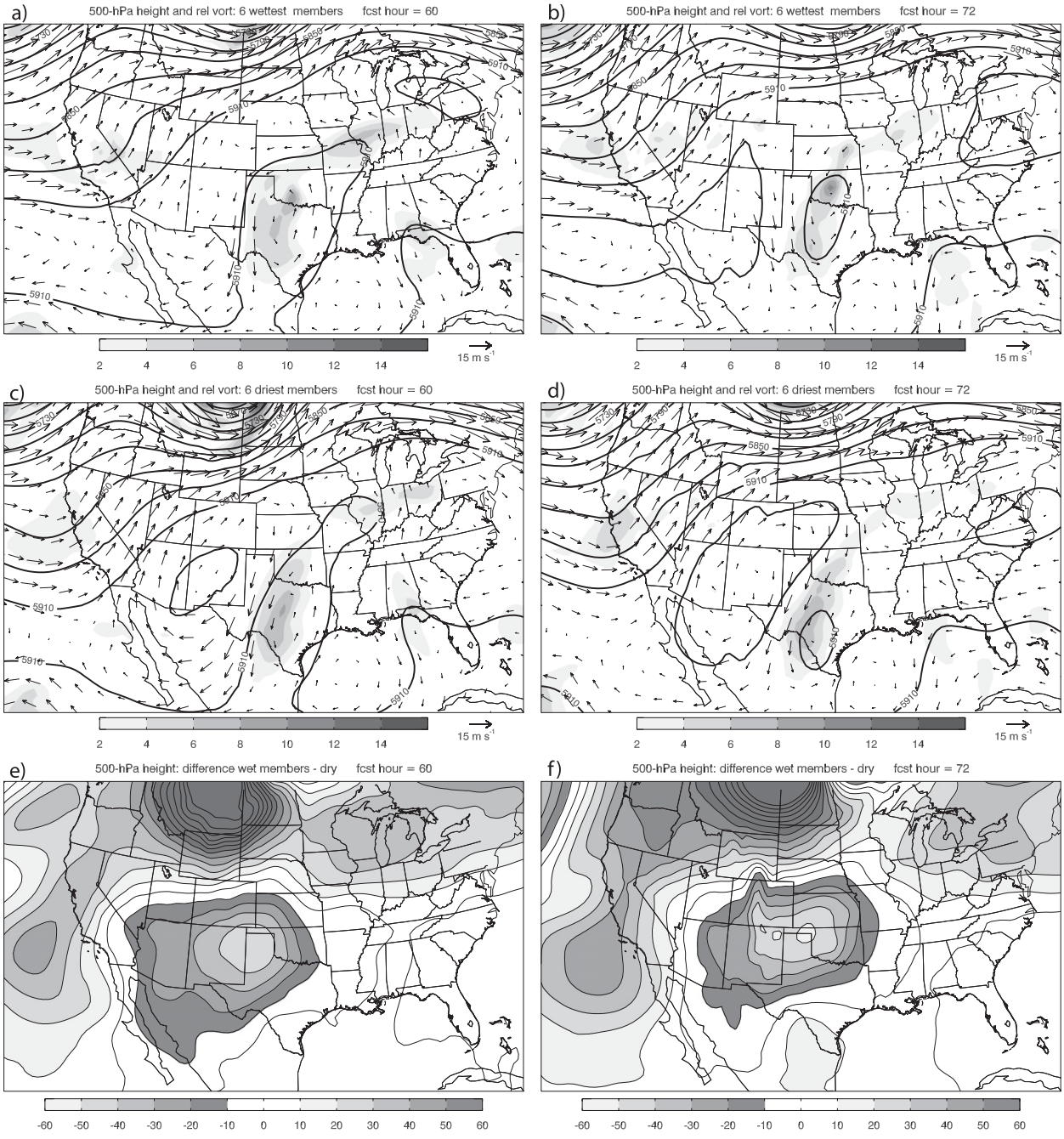

FIG. 15. As in Fig. 14, but for (a),(c),(e) forecast hour 60 (valid 1200 UTC 26 Jun) and (b),(d),(f) forecast hour 72 (valid 0000 UTC 27 Jun).

illustrate that, by hour 96, the earlier differences in the mass and wind fields have led to vastly different results, with a strong vortex over Oklahoma and Kansas in member 2 (Fig. 17a) that resembles the analysis at this time (Fig. 4f), and a decaying vortex over Mexico with an anticyclone over the southern plains in member 25 (Fig. 17b). In member 2 (and other wet ensemble members), the vortex remains over the southern plains for the next several days and has heavy rainfall associated with it, whereas the members in which the vortex was swept into Mexico have little precipitation in the subsequent days. The resulting precipitation accumulation between these two members is thus very different (cf. Figs. 5a and 5d), with comparable differences also

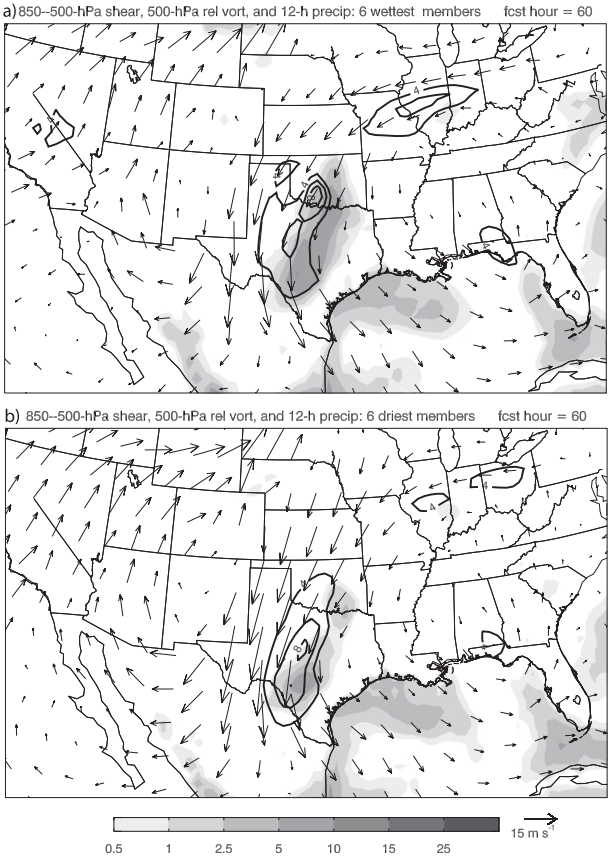

FIG. 16. The 500-hPa relative vorticity (contoured every 2×10^{-5} s^{-1} starting at 4), 850–500-hPa shear vectors, and precipitation (mm, shaded) in the 12 h ending at forecast hour 60 (1200 UTC 26 Jun) for the (a) wet and (b) dry composites.

occurring among the other individual members in the composites (not shown). The primary factors discriminating the ensemble members that developed a long-lived vortex and widespread rainfall over the southern plains from those that did not are summarized in Fig. 18.

c. *Smaller-scale factors*

The presentation above focused mainly on factors that were highlighted by correlations between synoptic-scale fields and *P*. However, there were some ensemble members that had very similar large-scale characteristics, yet nonetheless resulted in different rainfall totals over the southern plains. This is illustrated in Fig. 11, where at low values of vertical shear, some members had *P* exceeding 60 mm and some only around 40 mm. The differences between these members will be investigated in this section.

Three ensemble members with synoptic-scale patterns that at early times were generally similar to, but resulted in much less precipitation than, the ''best'' ensemble members are shown in Fig. 19. These three members had far more precipitation than the ''worst'' ensemble members shown in Figs. 5b and 5d, but not the extreme amounts in Figs. 5a and 5c or in observations. At forecast hour 60, these members had weak northerly 500-hPa flow over the north side of the vortex, similar to the wet composite and in contrast to the dry composite at this time (cf. Figs. 20a,c,e and Figs. 15a,c). Despite these similarities, however, the forecasts from these members diverge with time. Member 23 proceeds in a manner different from either the wet or dry composite, as a deep trough develops off the coast of California (Fig. 20d). A series of short-wave troughs, associated with deep convection, move eastward ahead of this trough, and the developing vortex moves eastward in the relatively strong westerly flow and does not remain over the southern plains (not shown). The differences between ensemble member 3 (Fig. 19a) and the wet members are more subtle. At forecast hour 96 (Fig. 20b),

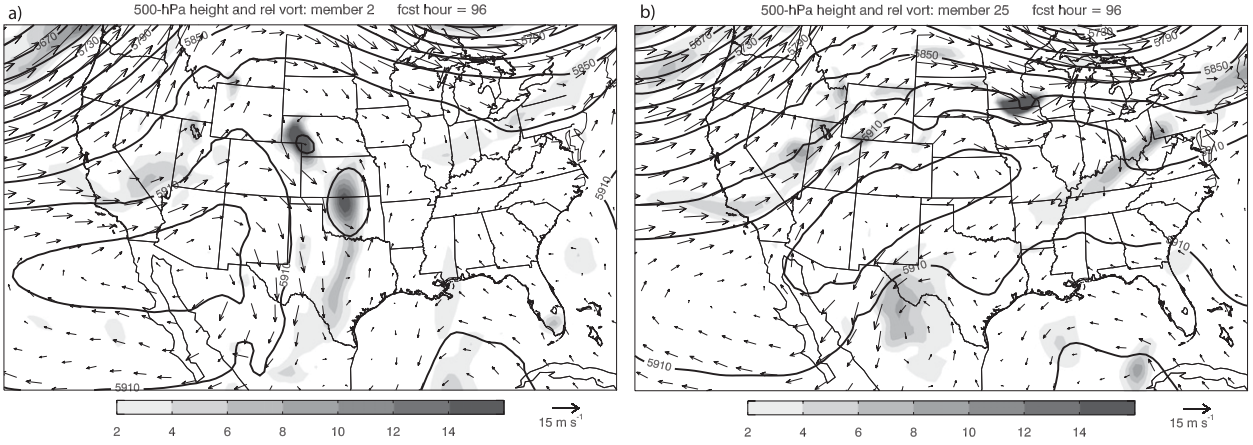

FIG. 17. As in Fig. 14a, but for individual ensemble members (a) 2 and (b) 25 at forecast hour 96 (0000 UTC 28 Jun).

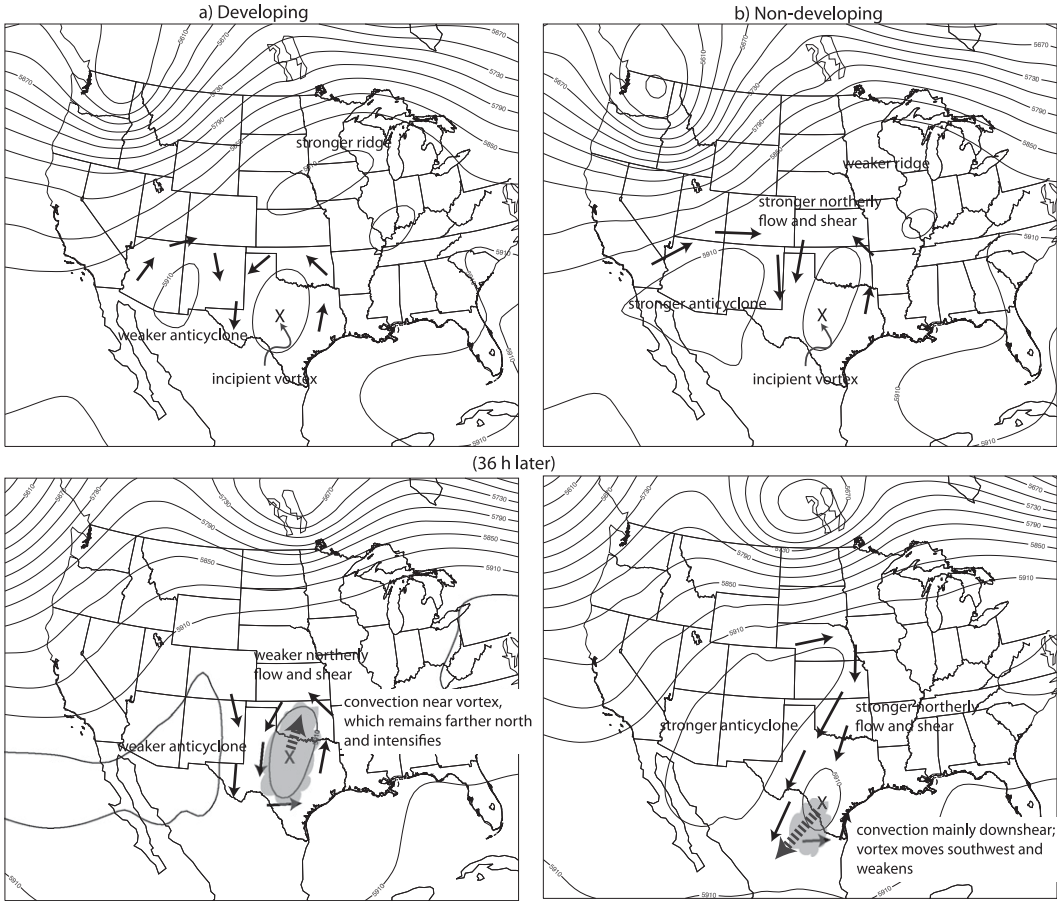

FIG. 18. Schematic diagram illustrating the large-scale factors leading to (a) development and (b) nondevelopment of a long-lived vortex and associated widespread rainfall, as indicated by differing ensemble members. The 500-hPa height patterns at an earlier time, and 36 later, are shown for both instances. Black arrows denote representative flow vectors. The × indicates the location of the 500-hPa vorticity maximum, gray shading indicates the location of deep convection, and the dotted arrow indicates the movement of the vortex over time.

a strong vortex has developed, but it is located over west-central Texas, slightly farther south than the observed vortex at this time. The vortex in this member moves slowly to the southwest and maintains its intensity, but with the result being erroneous heavy precipitation over south Texas (Fig. 19a). Member 45 follows a similar path as member 3 (Figs. 20e and 20f), but the convection near the vortex is weaker (not shown). The vortex in this member also drifts slowly southward, but weakens with time and dissipates completely by hour 108 (not shown). These three members illustrate the wide range of quantitative precipitation forecasts that result even with very similar synoptic-scale flow patterns at early times in the forecast.

5. Discussion

As discussed previously, there are some limitations to the analysis presented here. Because the initial ensemble perturbations are at large spatial scales, they then tend to project on large scales at later times as well. Thus, the ''failure modes'' for cyclogenesis and heavy rainfall suggested in Fig. 18b and section 4c may not be the *only* such failure modes for an event such as this. It has been established that small-scale errors owing to moist convection are also often responsible for large-scale errors at later times (e.g., Zhang et al. 2003), and since the ECMWF ensemble has relatively coarse resolution, it does not include some of these potential error sources at the smallest scales. Thus, this study provides a way of estimating the predictability of a widespread heavy rain event, but is not a comprehensive predictability analysis.

Nonetheless, the analysis in this study does provide some clues into the reasons for poor medium-range predictions of this event. Relatively small differences in the structure of the height and wind field in the southern United States translated into vastly different precipitation predictions over a large part of the country for

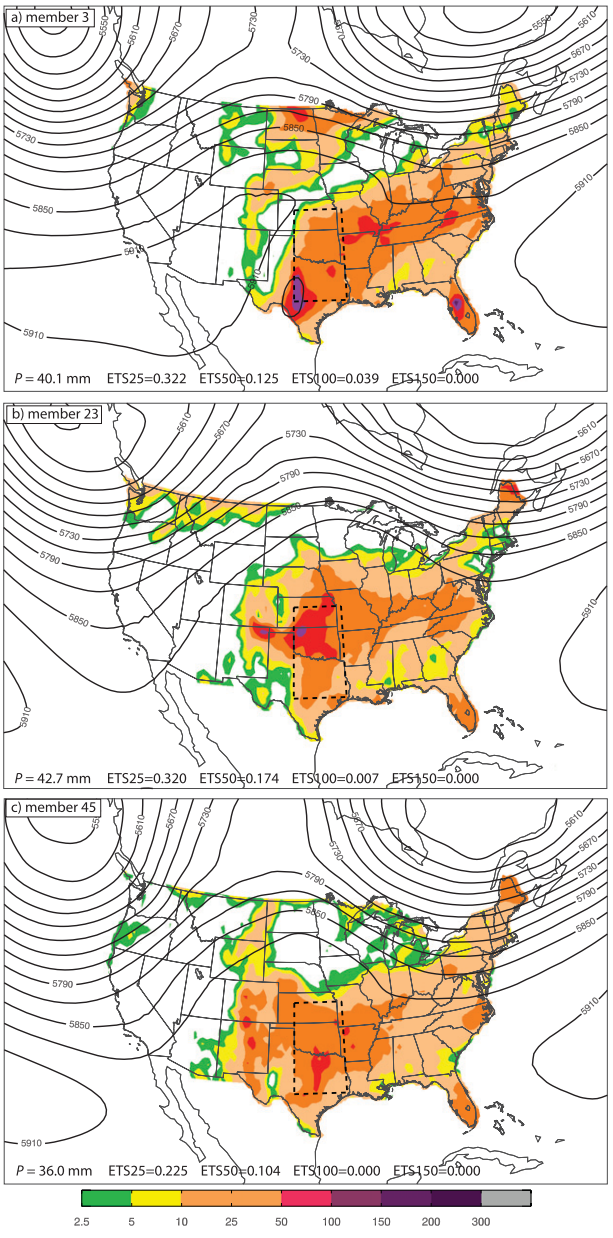

FIG. 19. As in Fig. 5, but for ensemble members (a) 3, (b) 23, and (c) 45.

many days. For forecasters and users alike, the proposition that the next week may bring anywhere from below normal precipitation to one of the wettest weeks on record in the warm season is not encouraging. In a broad-brush sense, global ensembles typically provide skillful forecasts at this range (e.g., Schumacher and Davis 2010), so the fact that there are some events with excellent forecasts and others with huge uncertainties creates a challenge for those communicating the forecasts and those trying to understand then.

The 500-hPa level has been the primary focus of the analysis here, both for the sake of simplicity in presentation and because it is generally the level with the highest correlations to later precipitation of the levels available. Of course, the patterns reflected at 500 hPa are also related to features in the lower and upper troposphere. For example, the development of the vortex and heavy precipitation is also associated with a slightly more amplified pattern on the dynamic tropopause, with a higher-amplitude ridge over the central United States and the eventual progression of a deeper trough over the western United States (not shown). Furthermore, there appears to be a connection between the location of the low-level baroclinic zone that was located across the eastern United States and the resulting precipitation, though this relationship is less straightforward than that demonstrated in the midlevel height and wind fields.

An event such as this also points toward other avenues of research. Aside from other documented examples such as the case described by Nielsen-Gammon et al. (2005), Zhang et al. (2006), and Knebl Lowrey and Yang (2008), it is not known how often these slow-moving, multiple-day vortices have occurred in the past, so an examination of climatological data for these events is warranted. Also, given the great sensitivity to small changes in the synoptic environment in this case, it is likely that there are many past instances where conditions were similar to those in June 2007 but long-lived circulations failed to develop. Further analysis of both developing and nondeveloping cases in the past would help to generalize, or refute, the findings of this study. This ensemble-based analysis also only scratches the surface of the dynamics of long-lived, nearly stationary continental vortices and their relationships to the synoptic-scale flow, which could be examined more fully with numerical experiments. In particular, the similarities and differences between this type of vortex and the genesis of a tropical cyclone over water remain open to investigation, and the importance of deep convection in maintaining the vortex over the southern plains has not been quantified. The development of surface fronts in association with a long-lived MCV has been documented by Galarneau et al. (2009), and the dynamical similarities between their case and this one could also be examined.

6. Conclusions

In this study, global ensemble forecasts are used to investigate the processes responsible for the development and maintenance of a multiple-day rain event that occurred in late June 2007. This event was previously shown to be poorly predicted at the medium range

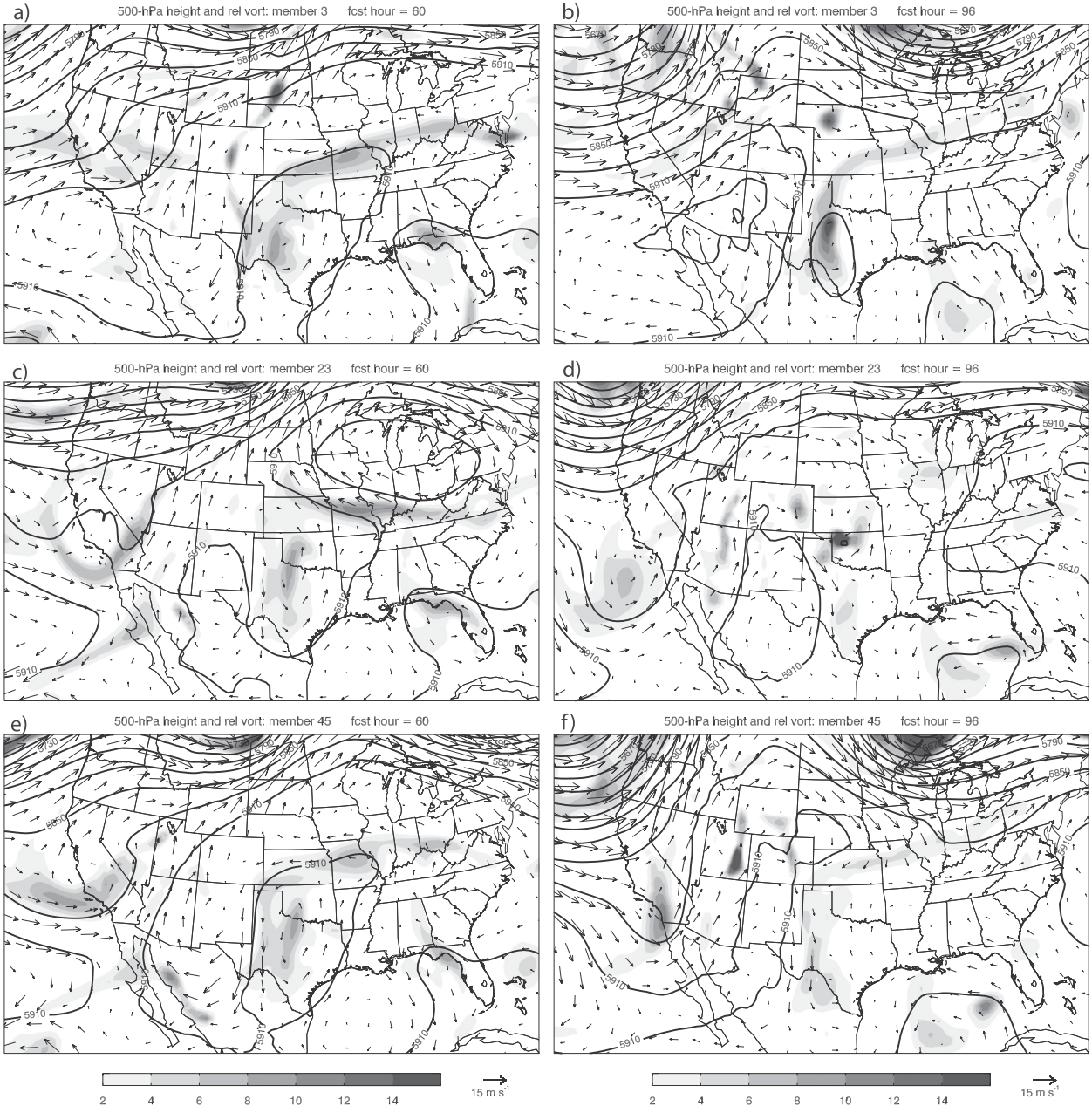

FIG. 20. As in Fig. 14a, but for individual ensemble members (a),(b) 3, (c),(d) 23, and (e),(f) 45 at forecast hours (a),(c),(e) 60 and (b),(d),(f) 96.

relative to other events of similar spatial and temporal scales, with low skill and large spread in ensemble forecasts. The heavy rainfall was associated with a long-lived warm-core vortex over the southern plains of the United States, and the ensemble quantitatively demonstrates the close connection between this vortex and the accumulated precipitation. Linear statistics are calculated to examine the atmospheric structures that favored or inhibited the development of the vortex and associated rainfall. The strength of a midtropospheric anticyclone in the southwestern United States was closely related to the later development of the vortex. A weaker anticyclone, which was also associated with weaker northerly wind shear over the incipient vortex, was favorable for development. In the ensemble members with a weaker anticyclone in the southwest United States, convection developed near the vortex center, and the vortex intensified and remained nearly stationary. In

the members with a stronger anticyclone, on the other hand, convection primarily occurred downshear of the vortex center and the circulation moved southwest into Mexico and eventually dissipated. These relatively small initial differences in the tropospheric mass and wind fields ultimately resulted in vastly different forecasts of precipitation over the southern plains. This strong sensitivity to small differences in the initial conditions underscores the importance of using ensembles for predicting the development of warm-core vortices over both land and ocean.

Acknowledgments. The ECMWF ensemble forecast data were obtained from the TIGGE archive online (http://tigge-portal.ecmwf.int). NARR data were obtained from NCEP, NCEP–NCAR reanalysis data were obtained from the NOAA/ESRL Physical Sciences Division, Boulder, Colorado, from their Web site (http://www.esrl.noaa.gov/psd/), and precipitation data were obtained from the NOAA Climate Prediction Center. The author wishes to thank Chris Davis for his mentorship, and NCAR for their postdoctoral support during early stages of this work. Thanks also go to Lance Bosart, Jason Sippel, John Nielsen-Gammon, and two anonymous reviewers for their constructive comments on an earlier version of this manuscript, and to Tom Hamill, David Dowell, Josh Hacker, and Tom Galarneau for helpful suggestions and discussions related to this work. This research was supported by National Science Foundation Grant AGS-0954908.

REFERENCES

Bosart, L. F., and F. Sanders, 1981: The Johnstown flood of July 1977: A long-lived convective system. *J. Atmos. Sci.,* **38,** 1616–1642.

Bougeault, P., and Coauthors, 2010: The THORPEX Interactive Grand Global Ensemble. *Bull. Amer. Meteor. Soc.,* **91,** 1059–1072.

Bracken, W. E., and L. F. Bosart, 2000: The role of synoptic-scale flow during tropical cyclogenesis over the North Atlantic Ocean. *Mon. Wea. Rev.,* **128,** 353–376.

Buizza, R., J.-R. Bidlot, N. Wedi, M. Fuentes, M. Hamrud, G. Holt, and F. Vitart, 2007: The new ECMWF VAREPS (Variable Resolution Ensemble Prediction System). *Quart. J. Roy. Meteor. Soc.,* **133,** 681–695.

Chen, M., W. Shi, P. Xie, V. B. S. Silva, V. E. Kousky, R. W. Higgins, and J. E. Janowiak, 2008: Assessing objective techniques for gauge-based analyses of global daily precipitation. *J. Geophys. Res.,* **113,** D04110, doi:10.1029/2007JD009132.

Davis, C. A., and L. F. Bosart, 2004: The TT problem: Forecasting the tropical transition of cyclones. *Bull. Amer. Meteor. Soc.,* **85,** 1657–1662.

ECMWF, cited 2010a: The creation of perturbed analyses. [Available online at http://www.ecmwf.int/products/forecasts/guide/The_creation_of_perturbed_analyses.html.]

——, cited 2010b: Total column water. [Available online at http://tigge.ecmwf.int/tigge/d/show_object/table=parameters/name=total_column_water/levtype=sfc/.]

Fritsch, J. M., J. D. Murphy, and J. S. Kain, 1994: Warm-core vortex amplification over land. *J. Atmos. Sci.,* **51,** 1780–1807.

Galarneau, T. J., Jr., L. F. Bosart, C. A. Davis, and R. McTaggart-Cowan, 2009: Baroclinic transition of a long-lived mesoscale convective vortex. *Mon. Wea. Rev.,* **137,** 562–584.

Goebbert, K. H., A. D. Schenkman, C. M. Shafer, and N. A. Snook, 2008: An overview of the summer 2007 excessive rain event in the southern plains. Preprints, *22nd Conf. on Hydrology,* New Orleans, LA, Amer. Meteor. Soc., P1.2. [Available online at http://ams.confex.com/ams/pdfpapers/135330.pdf.]

Gray, W. M., 1968: Global view of the origin of tropical disturbances and storms. *Mon. Wea. Rev.,* **96,** 669–700.

Hakim, G. J., and R. D. Torn, 2008: Ensemble synoptic analysis. *Synoptic-Dynamic Meteorology and Weather Analysis and Forecasting: A Tribute to Fred Sanders, Meteor. Monogr.,* No. 55, Amer. Meteor. Soc., 147–161.

Hamill, T. M., and J. Juras, 2006: Measuring forecast skill: Is it real skill or is it the varying climatology? *Quart. J. Roy. Meteor. Soc.,* **132,** 2905–2923.

Hawblitzel, D. P., F. Zhang, Z. Meng, and C. A. Davis, 2007: Probabilistic evaluation of the dynamics and predictability of the mesoscale convective vortex of 10–13 June 2003. *Mon. Wea. Rev.,* **135,** 1544–1563.

Haynes, P. H., and M. E. McIntyre, 1987: On the evolution of vorticity and potential vorticity in the presence of diabatic heating and frictional or other forces. *J. Atmos. Sci.,* **44,** 828–841.

Hennon, C. C., and J. S. Hobgood, 2003: Forecasting tropical cyclogenesis over the Atlantic basin using large-scale data. *Mon. Wea. Rev.,* **131,** 2927–2940.

James, E. P., and R. H. Johnson, 2010: Patterns of precipitation and mesolow evolution in midlatitude mesoscale convective vortices. *Mon. Wea. Rev.,* **138,** 909–931.

Kalnay, E., and Coauthors, 1996: The NCEP/NCAR 40-Year Reanalysis Project. *Bull. Amer. Meteor. Soc.,* **77,** 437–471.

Kerns, B., and E. Zipser, 2009: Four years of tropical ERA-40 vorticity maxima tracks. Part II: Differences between developing and nondeveloping disturbances. *Mon. Wea. Rev.,* **137,** 2576–2591.

Knebl Lowrey, M. R., and Z.-L. Yang, 2008: Assessing the capability of a regional-scale weather model to simulate extreme precipitation patterns and flooding in central Texas. *Wea. Forecasting,* **23,** 1102–1126.

Koch, S. E., M. desJardins, and P. J. Kocin, 1983: An interactive Barnes objective map analysis scheme for use with satellite and conventional data. *J. Climate Appl. Meteor.,* **22,** 1487–1503.

McBride, J. L., and R. Zehr, 1981: Observational analysis of tropical cyclone formation. Part II: Comparison of non-developing versus developing systems. *J. Atmos. Sci.,* **38,** 1132–1151.

Mesinger, F., and Coauthors, 2006: North American Regional Reanalysis. *Bull. Amer. Meteor. Soc.,* **87,** 343–360.

Nielsen-Gammon, J. W., F. Zhang, A. M. Odins, and B. Myoung, 2005: Extreme rainfall in Texas: Patterns and predictability. *Phys. Geogr.,* **26,** 340–364.

NOAA, 2007: *Storm Data*. Vol. 49, No. 8, 530 pp.

Park, Y. Y., R. Buizza, and M. Leutbecher, 2008: TIGGE: Preliminary results on comparing and combining ensembles. *Quart. J. Roy. Meteor. Soc.,* **134,** 2029–2050.

Schumacher, R. S., and R. H. Johnson, 2008: Mesoscale processes contributing to extreme rainfall in a midlatitude warm-season flash flood. *Mon. Wea. Rev.,* **136,** 3964–3986.

——, and C. A. Davis, 2010: Ensemble-based forecast uncertainty analysis of diverse heavy rainfall events. *Wea. Forecasting,* **25,** 1103–1122.

Schumacher, A. B., M. DeMaria, and J. A. Knaff, 2009: Objective estimation of the 24-h probability of tropical cyclone formation. *Wea. Forecasting,* **24,** 456–471.

Sippel, J. A., and F. Zhang, 2008: A probabilistic analysis of the dynamics and predictability of tropical cyclogenesis. *J. Atmos. Sci.,* **65,** 3440–3459.

——, and ——, 2010: Factors affecting the predictability of Hurricane Humberto (2007). *J. Atmos. Sci.,* **67,** 1759–1778.

Torn, R. D., 2010: Diagnosis of the downstream ridging associated with extratropical transition using short-term ensemble forecasts. *J. Atmos. Sci.,* **67,** 817–833.

Trier, S. B., C. A. Davis, and J. D. Tuttle, 2000: Long-lived mesoconvective vortices and their environment. Part I: Observations from the central United States during the 1998 warm season. *Mon. Wea. Rev.,* **128,** 3376–3395.

Zhang, F., C. Snyder, and R. Rotunno, 2003: Effects of moist convection on mesoscale predictability. *J. Atmos. Sci.,* **60,** 1173–1185.

——, A. M. Odins, and J. W. Nielsen-Gammon, 2006: Mesoscale predictability of an extreme warm-season precipitation event. *Wea. Forecasting,* **21,** 149–166.